Atmospheric Research 190 (2017) 43–54

Contents lists available at ScienceDirect

Atmospheric Research

journal homepage: www.elsevier.com/locate/atmosres

Assessment of satellite precipitation estimates over the slopes of the subtropical Andes

María Paula Hobouchian [a,*], Paola Salio [b,c,d], Yanina García Skabar [a,e,d], Daniel Vila [f], Rene Garreaud [g]

[a] Departamento de Investigación y Desarrollo, Servicio Meteorológico Nacional, Argentina
[b] Centro de Investigaciones del Mar y la Atmósfera, CONICET UBA, Argentina
[c] Departamento de Ciencias de la Atmósfera y los Océanos, FCEyN, Universidad de Buenos Aires, Argentina
[d] UMI-Instituto Franco Argentino sobre Estudios del Clima y sus Impactos, Argentina
[e] CONICET, Argentina
[f] División de Satélites y Sistemas Ambientales, CPTEC, Brazil
[g] Departamento de Geofísica, Universidad de Chile, Chile

ARTICLE INFO

Article history:
Received 16 August 2016
Received in revised form 4 January 2017
Accepted 6 February 2017
Available online 16 February 2017

Keywords:
Precipitation
Satellite products
Topography

ABSTRACT

A validation of four satellite daily precipitation estimates at a spatial resolution of 0.25° is performed over the subtropical Andes, an area of highly complex topography: The Tropical Rainfall Measuring Mission (TRMM) Multisatellite Precipitation Analysis (TMPA, 3B42 V7 and RT), the Climate Prediction Center Morphing technique (CMORPH) and the Hydro-Estimator (HYDRO). Remote mountainous regions represent a major challenge for these satellite data products and for studies examining their quality with surface data.

For the assessment of the satellite products, a period of seven years from January 1st 2004 to December 31st 2010 was considered. Different statistics were analyzed considering their variability in the study area and identifying their main differences between the warm and cold seasons. The results indicate a decrease in winter errors which coincides with the wet season over the windward side of the Andes. Also, a significant underestimation of precipitation is observed for all estimates throughout the period analyzed.

The analysis with respect to terrain height shows a greater dependence of errors with topography for all the algorithms that combine infrared and passive microwave data, HYDRO providing the most stable result. The main limitations of the estimates associated with the type of precipitating event and their location relative to the orography are assessed.

Finally, the analysis of two intense precipitation events is presented and allows the assessment of the latest advances in satellite derived estimates with the launch of the Global Precipitation Measurement.

1. Introduction

Precipitation has a fundamental role in regulating the hydrological cycle, as well as different socio-economic activities. For this reason, accurate precipitation measurements provide important information for decision-making (Kucera et al., 2013). In South America, the available rainfall network has significant limitations in its infrastructure, maintenance, density and frequency of observations.

Satellite Precipitation estimates continue to be an ongoing challenge today. Passive microwave (PM) measurements are capable of inferring the internal structure of clouds generally providing higher quality precipitation estimates than the algorithms based on visible (VI) or infrared (IR) data on the global scale (Ebert et al., 2007). However, the advantage of using IR precipitation estimates from geostationary satellites is that they have a higher temporal resolution, and a nearly global coverage. Precipitation products derived from combining IR observations with PM observations, known as "blended techniques," perform better in the global context (Ebert et al., 2007). Some algorithms further consider active microwave data and surface information in the calibration procedure (Huffman et al., 2007; Vila et al., 2009; Kidd and Levizzani, 2011). An updated list of the available precipitation estimations is presented in Table 2 in Tapiador et al. (2012).

The most recognized precipitation estimates include: the Climate Prediction Center Morphing Method (CMORPH; Joyce et al., 2004); the Multi-satellite TRMM Precipitation Analysis (TMPA, known as 3B42; Huffman et al., 2007); the Global Satellite Mapping of Precipitation (GSMaP; Okamoto et al., 2005); the Hydro-Estimator (HYDRO, Scofield and Kuligowski, 2003); the Remotely Sensed Precipitation Estimation from Information using Artificial Neural Networks (PERSIANN; Sorooshian et al., 2000); local developments in South America such as the Combined Scheme (CoSch; Vila et al., 2009); and the recent developments exploiting the new Global Precipitation Measurement (GPM)

* Corresponding author at: Departamento de Investigación y Desarrollo, Servicio Meteorológico Nacional, Av. Cnel. M. Dorrego 4019, C1425GBE Buenos Aires, Argentina.
E-mail address: phobouchian@smn.gov.ar (M.P. Hobouchian).

http://dx.doi.org/10.1016/j.atmosres.2017.02.006
0169-8095/

mission, namely the Integrated Multi-Satellite Retrievals for the Global Precipitation Measurement mission (IMERG, Huffman et al., 2015).

Globally, the performance of retrieval algorithms is highly dependent on surface conditions, latitude and season. South America, a region that experiences some of the most intense mesoscale convective systems (MCSs) on Earth (Zipser et al., 2006), has areas of complex topography (i.e., the Andes range), snow-covered surfaces, and heavy precipitation from warm clouds in areas such as northeastern Brazil and the Amazon (Liu and Zipser, 2009).

Salio et al. (2015) advanced on determining the quality of satellite rainfall estimates over South America by evaluating them over a dense rain gauge network providing 24-hour accumulation information. Precipitation estimates that included microwave data showed a remarkable performance, which was shown to improve further by including surface observations. In the south of South America, CoSch departed favorably from the rest of the estimates, and 3B42 V7 improved over 3B42 V6, 3B42 RT and CMORPH showed a greater degree of overestimation for the most intense precipitation events, and HYDRO showed an underestimation in all seasons and in most of the thresholds. The errors were minimal in the northeastern region of Argentina and in southeastern Brazil, mainly affected by convective precipitation. The greatest difficulties were shown to arise in mountainous areas and in non-convective precipitation events. Particularly, over the subtropical Andes, the persistence of underestimated precipitation estimates was observed.

Complex topography presents additional challenges for satellite rainfall retrievals. The main problem is the lack of rain gauge observations over mountainous regions. In recent years, scientific research has focused on evaluating the performance of satellite precipitation estimates in different mountainous regions (Dinku et al., 2008, 2010, 2011, Hirpa et al., 2010; Habib et al., 2012, Gao and Liu, 2012, Blacutt et al., 2015, Salio et al., 2015).

Dinku et al. (2010) validated seven satellite precipitation estimates on a daily time scale for an area of complex topography in Colombia. The products showed overestimations in both rainfall amount and occurrence over the relatively dry northern region and significant underestimations over the mountainous regions and the Pacific coast. The best performance was achieved over the eastern plains of Colombia, and the performance of the products was relatively poor over the Pacific coast. The overestimation over the northern region has been associated to possible subcloud evaporation, and the underestimations observed over the mountainous and coastal regions may be associated with warm-rain processes. Similar results were found over the highlands of Ethiopia in a study that focused on the mountainous and arid regions of east Africa (Dinku et al., 2011; Dinku et al., 2008). The daily validation over complex terrain in Africa (Dinku et al., 2008) showed that CMORPH and 3B42 RT perform reasonably well in detecting the occurrence of rainfall. However, their performance is poor in estimating the amount of rainfall in each pixel. In this line, Hirpa et al. (2010) made an Evaluation of High-Resolution Satellite Precipitation Products over Very Complex Terrain in Ethiopia. 3B42 RT and CMORPH showed similar rainfall results but showed an elevation-dependent trend. IR based rainfall algorithms have also shown major limitations in reproducing rainfall fields in mountainous regions of East Africa, considerably underestimating rainfall in high-elevation areas.

Gao and Liu (2012) carried out a daily evaluation of the performance of CMORPH and 3B42 V6 on the Tibetan Plateau, and showed the 3B42 V6 outperformed CMORPH due to its monthly surface data adjustment. Products were shown to overestimate weak precipitation and underestimate moderate to strong rainfall over the threshold of 10 mm per day. Gao and Liu (2012) further noted that products that depend heavily on microwave data produce better precipitation estimates in complex terrain regions than PERSIANN that relies primarily on IR data. The results were further analyzed by differentiating between dry and wet regions by taking into account land elevation. PERSIANN showed a marked difference in the underestimation of precipitation events at lower altitudes and the overestimation of precipitation events at higher elevations. The products derived from the added combination of PM data do not show such dependence in terrain elevation, which also show better results in the statistical data of the wetlands of the Tibetan plateau compared to the more arid regions.

A comparison for the 3B42 V7 and CoSch datasets was performed by Blacutt et al. (2015) for the rainy and dry seasons over Bolivia. These products exhibit underestimated heavy rainfall (>50 mm day^{-1}) on both rainy and dry seasons and overall, the outcome of combining 3B42 V7 with the surface observations is shown to be positive over this complex terrain region.

The main limitations of satellite precipitation estimation in mountainous regions arise from the underestimation of precipitation from warm clouds, the underestimation of very heavy rainfall without an internal structure of ice crystals, the overestimation on snow-covered surfaces, and the overestimation generated by evaporation of rainfall below the cloud base before reaching the surface, the latter difficulty increasing in the more arid regions. Warm clouds lack sufficient vertical growth to reach low cloud top temperatures that are used as thresholds in IR retrieval algorithms. Heavy rainfall lacking a vertical structure of densely populated frozen hydrometeors fails to produce the scattering signals used in microwave retrieval algorithms while snow-covered regions can be mistaken for precipitation in microwave retrieval algorithms.

The Subtropical Andes (30–40°S) divide the areas of central Chile and west-central Argentina. It is of great interest to advance in the understanding of precipitation events that develop in this remote region characterized by a lack of observations. Satellite derived precipitation data is thus a crucial tool for hydrological applications, water management and decision-making in the region.

The present study extends the comprehensive evaluation of the performance of satellite precipitation estimates over southern South America conducted by Salio et al. (2015) over a longer period of time (to cover 7 years) in order to focus on mountainous regions, specifically over the subtropical Andes. This study proposes a systematic evaluation of 24 h precipitation accumulation periods in relation to terrain complexity and the differences between the warm and cold seasons.

This paper is organized as follows: Section 2 presents the validation region and the rain gauge data used. Section 3 presents the satellite precipitation estimates used. The methodology is detailed in Section 4, and results of the product intercomparison are presented in Sections 5 and 6. Finally, the discussion and conclusions are presented in Section 7.

2. Study region and rain gauge data

The present study was conducted over a common period of 7 years, from January 1st, 2004 to December 31st, 2010. Fig. 1 shows the region analyzed denoted by a box which covers the subtropical Andes range in Argentina and Chile, and the complex terrain at the spatial resolution of the satellite estimates. Fig. 2 shows the percentage of the days with data and the number of rain gauges available in each 0.25° latitude by 0.25° longitude area. To achieve the most representative and consistent data for verification, only grid points that have information for at least 70% of the days were taken into account for the selected period. The available network is unevenly distributed over 230 grid points.

This study considers 24-hour accumulated precipitation at 12 UTC. Precipitation measurements on the Argentinean side of the Andes are determined from heated rain gauges during the winter to measure snowfall inside mountain valleys and regular rain gauges at low elevation areas. On the Chilean side of the Andes, standard rain gauges (mostly Hellmann type or similar) with no heating are available. Although the non-heated instrument may have some problems during snow storms, nearly all stations in Chile are located below 2000 m above sea level and they hardly receive solid precipitation.

The methods used to grid the observations to match rain gauge and satellite data have several problems, and many studies show that there is no single algorithm that outperforms in all conditions. In areas with

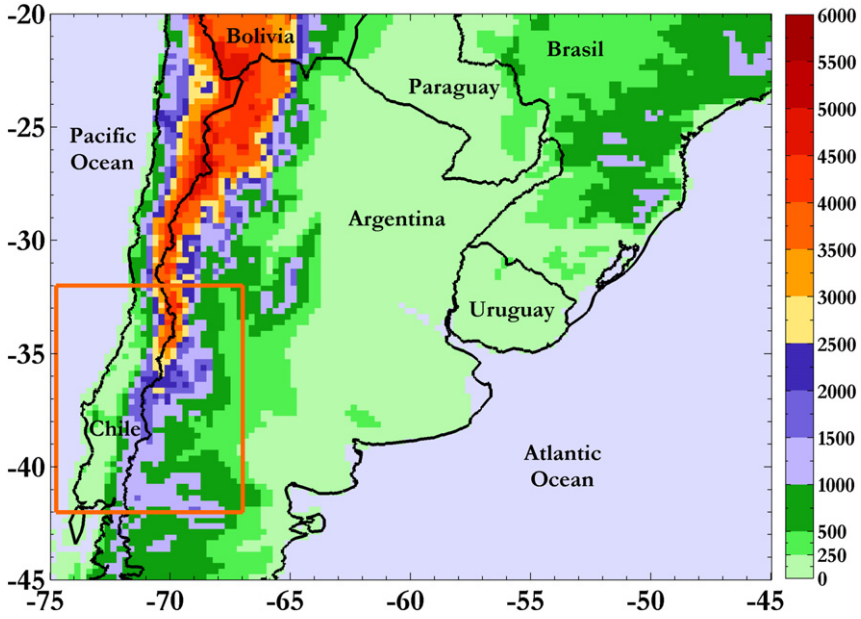

Fig. 1. Topography over southern South America in the grid of 0.25° spatial resolution matching estimates (shaded); and the study area over the subtropical Andes (orange outline). Terrain elevation is in meters.

unequally distributed sparse rain gauges, the analysis of different rain gauges will provide similar results (Ebert et al., 2007; Porcu et al., 2014). In the present study, data is interpolated to a 0.25° resolution grid by averaging the available data over each 0.25° × 0.25° area and assigning the mean value to the center of the grid. This methodology had been applied by Liebmann and Allured (2005) who obtained good results for their region of interest. In the same way, Demaria et al. (2011) indicated that the impact of the interpolation method does not have an effect on the results of a similar study over southeastern South America.

A quality control was performed on the observations. It consisted on the detection of errors in the registered date, the elimination of negative precipitation values, and the analyses of extremes, contiguous values and days without precipitation. Extreme events were analyzed on a case-by-case basis to identify incorrect data. For this task, thresholds related to the known precipitation regime of the region were set and atypical cases were carefully examined with information from the nearest weather stations and surrounding weather conditions. In addition, daily precipitation time series were used to compare the rainfall data and the different estimates in the most complex situations. The purpose of this process was to make a decision about removing or maintaining the analyzed data. If the data were removed, it was considered as missing information, without applying any interpolation methodology for missing data.

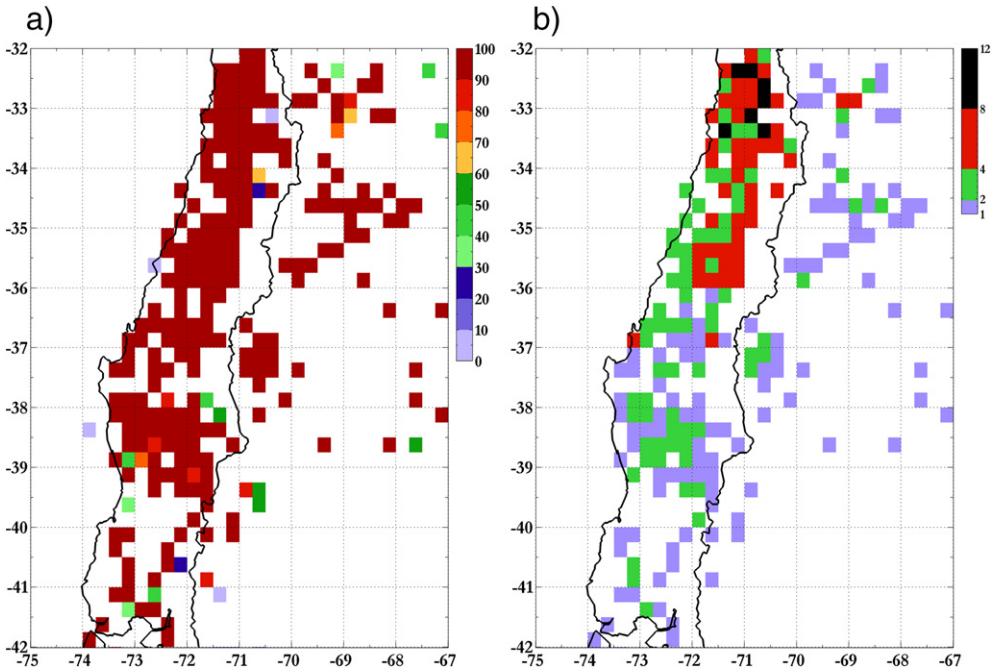

Fig. 2. (a) Percentage of days with available data and (b) number of rain gauges on each 0.25° interpolated spatial resolution grid with at least 70% of days with data for the period 2004–2010.

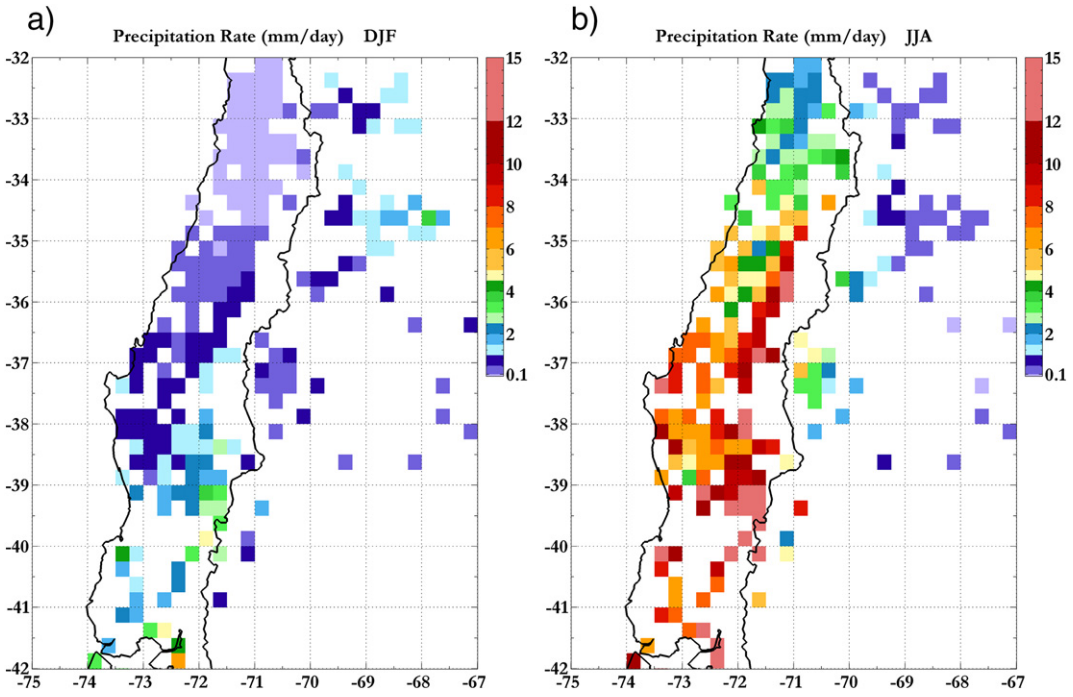

Fig. 3. Daily rate of rainfall precipitation (mm day^{-1}) at each grid point with at least 70% of days with data during the seasons (a) DJF summer, and (b) JJA winter over the subtropical Andes.

The precipitation regime in the study region is very different between summer and winter. Fig. 3 shows the daily rate of rainfall precipitation for the quarter December-January-February (DJF) and June-July-August (JJA) at each available grid point. In the subtropical Andes, rainfall occurs mainly in winter, often in the form of snow, which develops in the windward side of the Andes and on the high peaks. In the region near 35°S, the accumulated annual rainfall is <500 mm and is mainly generated by the entrance of cold fronts and occasional episodes of rainfall below the 0 °C isotherm (Garreaud, 2013; Viale and Nuñez, 2011). In summer, precipitation occurs mainly on the Argentinean side of the Andes and has a convective character, with very intense storms capable of developing large hail (Sanchez et al., 2011; Rosenfeld et al., 2006), mainly to the south of the study area (Viale and Garreaud, 2014).

3. Satellite precipitation estimates

Table 1 summarizes the main characteristics of the satellite precipitation estimates used, i.e. the resolution, type, coverage and periods of availability.

Three satellite-derived microwave precipitation products were analyzed in this study: CMORPH, TRMM 3B42 in its real time version (3B42 RT), and TRMM 3B42 in its research version 7 (3B42 V7). All estimations have a 0.25° spatial resolution and a 3-hour temporal resolution.

There are methodological differences among the mentioned algorithms. CMORPH uses passive microwave data to estimate the associated rain rate with a morphing method, and IR data from geostationary satellites to estimate the motion of cloud systems with propagation vectors. The TRMM 3B42 RT algorithm combines all available microwave estimates through the "histogram matching" technique, and converts the brightness temperatures of the infrared channel into precipitation rates from calibrated microwave data. The TRMM 3B42 V7 adds Precipitation Radar data from the TRMM platform to calibrate microwave data and it is further corrected with monthly rain gauge data. These surface data available on the Global Telecommunication System were not used for validation in order to have independent databases. Improvements have been introduced in the 3B42 V7 algorithm as compared to the previous version available (3B43 V6), specifically, the consideration of microwave moisture soundings and uniformly reprocessed input data (Huffman and Bolvin, 2014). The Hydro-Estimator (HYDRO; Vila et al., 2002; Scofield and Kuligowski, 2003) is one of the available estimates that are based on thermal IR brightness temperatures from geostationary satellites and humidity correction factors from numerical models. The primary idea is that it relates a pixel of rain with cloud tops colder than the average environmental temperature. HYDRO is widely used in the region due to the rapid updates that IR sensors onboard geostationary satellites provide. The version used in the present study is available from the Centro de Previsão de Tempo e Estudos Climáticos (CPTEC), and data is available every 30 min with a spatial resolution of 4 km. It uses the CPTEC/ETA Regional Model output to improve its performance. Precipitable water and

Table 1
Information of the satellite precipitation estimates evaluated in the present study.

Estimate	Resolution	Type	Reference	Web-coverage-period
3B42 RT (NASA)	0.25°-3 h	IR-PMW	Huffman et al. (2007)	**ftp://disc2.nascom.nasa.gov/data/TRMM/Gridded/3B42RT/** (Global/2000-2010)
3B42 V7 (NASA)	0.25°-3 h	IR-PMW-PR OBS (monthly)	Huffman and Bolvin (2014)	**ftp://disc2.nascom.nasa.gov/data/TRMM/Gridded/3B42_V7/** (Global/1998-2010)
CMORPH (NOAA)	0.25°-3 h	IR-PMW	Joyce et al. (2004)	**ftp://ftp.cpc.ncep.noaa.gov/precip/global_CMORPH/** (Global/2002-2010)
HYDRO (CPTEC)	4 km-30 min	IR HR y PW (model)	Scofield and Kuligowski (2003)	**http://sigma.cptec.inpe.br/prec_sat/** (South America/2003–2010)

relative humidity between the surface and 500 hPa are used to adjust the relation between cloud-top temperature and precipitation rates. These adjustments decrease rainfall rates in very dry environments and increase them in very moist environments. Low-level winds and a digital elevation model are also used to improve rainfall retrievals over complex terrains (Vila et al., 2002; Vicente et al., 2001).

Taking into account the spatial resolution of the different estimates in comparison to the rain-gauge network available for the present study, a resolution of 0.25° is chosen for all estimates. This resolution is detrimental to HYDRO which has higher resolution, but most of the areas have only one station in the 0.25° grid box (Fig. 2) and a validation with higher resolution is not suitable.

In February 2014, the core of the GPM mission observatory was launched. This mission, carried out jointly between the National Aeronautics and Space Administration (NASA) and the Japan Aerospace Exploration Agency (JAXA), includes a constellation of international satellites. The main critical improvements it proposes in real-time are an increased coverage of latitude, the incorporation of dual frequency precipitation radar which improves the estimates on shape, size and distribution of the hydrometeors, and a microwave radiometer with high microwave frequency channels. These advances in available data will improve the detection of heavy rain, light rain and snow.

GPM data is now available from March 2014 to the present. The most complete precipitation estimate from the mission is the IMERG GPM product. This algorithm aims to calibrate, attach and interpolate precipitation estimates from microwave and IR data, rainfall rain gauge data and other potential precipitation estimates in an optimal manner with a resolution of 0.1° and at 30 min, and at a global coverage (60° N-S). The system operates several times in each observation time, providing a better estimate as it incorporates new information. In the final stage, monthly rain gauge data is used to create research products. A full description of the technical specifications of IMERG is provided by Huffman et al. (2015).

The IMERG estimate is provided with the versions of 3B42 until mid-2017 to secure a prudent transition between them. The IMERG data will be processed retrospectively (data 2000–present) in 2017, and this is the main reason why IMERG historical data was not included in the present work. Nonetheless, two events of intense precipitation in the study region were included and correspond to the dates April 8th and June 11th 2014, in order to conduct a comparison between IMERG, 3B42 V7 and rain gauge data. This provides further analysis in the quality improvements of the new algorithms.

4. Methodology

The statistical analysis conducted takes into account the whole period of study and the quarter December to February (DJF) and June to August (JJA).

The classical statistical indicators that were used are: the root mean square error, which provides a measure of the mean value of errors estimate, and the bias, which represents the systematic error of the estimates. Both statistics were normalized by the daily precipitation rate of the analyzed period to achieve comparable values for different seasons and regions following the methodology used by Su et al. (2008). In addition, the correlation coefficient (CORR), which represents the degree of linear association between estimates and observations, was calculated. The normalized root mean square error (NRMSE), the percent bias (BIAS%) and the correlation coefficient were calculated to evaluate the performance of the different estimates (Salio et al., 2015).

Categorical statistics, such as bias score (BIASS), equitable threat score (ETS), probability of detection (POD) and false alarms (FAR) were used for determining the quality of the estimates at different precipitation intervals. BIASS measures the relationship between the frequency of estimated precipitation events regarding observed precipitation events, and the perfect value is 1. POD describes the fraction of observed precipitation events that were estimated correctly, and the perfect value is 1. FAR complements the POD as it measures the fraction of estimated precipitation events that did not actually occur, and the perfect value is 0. ETS measures the fraction of precipitation events that were correctly estimated considering the number of random hits. Multiple precipitation thresholds have been considered to calculate the statistics: 0.5, 1, 2, 3, 4, 5, 6, 7, 8, 9, 10, 12, 15, 20, 30 and 50 mm, which were chosen as reported in different bibliographical references (Salio et al., 2015; Vila et al., 2009; Ruiz, 2009), with the aim of evaluating estimates across the different precipitation structures. The formal definitions of these skill indicators are included in the validation page http://www.cawcr.gov.au/projects/verification/ and in Nurmi (2003).

Table 2
Statistics for the different rainfall estimates in the entire study period 2004–2010 over the subtropical Andes. N represents the number of observation-estimate pairs available for daily validation.

$N = 576.272$	NRMSE	BIAS%	CORR
HYDRO	3,52	−43,20	0,36
CMORPH	3,38	−52,23	0,26
3B42 RT	3,54	−41,25	0,30
3B42 V7	3,67	−18,99	0,33

The probability distribution of precipitation volumes (PDF), suggested by Amitai et al. (2012), considers the relative contribution of each precipitation interval to the total precipitation volume. These PDFs are defined as the sum of all the precipitation rates for a given interval in the dBR scale (dBR = 10log(R/1 mm day^{-1}); [R] = [mm day^{-1}]) divided by the sum of all the precipitation rates:

$$\mathrm{PDF}(R_i) = \frac{\int_{R_i-0.5}^{R_i+0.5} R\,P(R)\,dR}{\int_0^{\infty} R\,P(R)\,dR} \quad (1)$$

where R represents the amount of rainfall in mm and P is the rainfall probability. These PDFs have the advantage of being less sensitive to limitations in detecting weak precipitation (associated with a small fraction of the total precipitation) compared with PDFs of occurrence, and for that reason are good for comparing surface observations with estimates derived from algorithms and instruments with different detection limits.

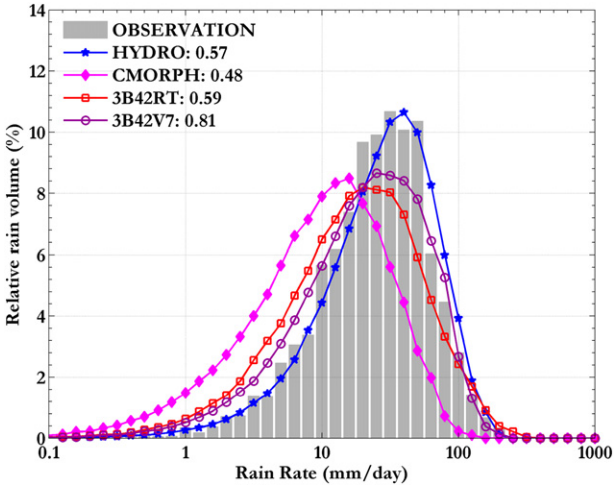

Fig. 4. Volumetric PDFs for the different precipitation estimates in the entire study period 2004–2010 over the subtropical Andes. The relation between the estimated total precipitation and the observed total precipitation in the area is indicated in the legend.

5. Assessment of the precipitation estimates over the subtropical Andes

The overall statistical results for the studied period are summarized in Table 2. The values are similar to those found by Salio et al. (2015) for a shorter 2 years period and for the same region, and complement this previous evaluation. Estimates show a marked underestimation in this region, with the lowest obtained BIAS% of −52.23 for CMORPH, which also exceeds 40% for HYDRO and 3B42 RT. The total NRMSE does not indicate large differences between the estimates and, in line with the result for BIAS%, CMORPH also has the worst correlation value. Meanwhile, 3B42 V7 reduces the level of underestimation with a BIAS% of −18.99 despite a slightly higher value in the NRMSE and intermediate correlation results, and it also achieves a significant improvement over 3B42 RT. HYDRO, despite a significant degree of underestimation, reduces the error value and increases the correlation with observations.

PDFs are shown in Fig. 4 and include in the legend the relation between the estimated total precipitation and the observed precipitation over the region and the entire study period. A ratio greater to one indicates an overestimation by the algorithm, and a ratio below one represents an underestimation. Furthermore, the curve of each estimate

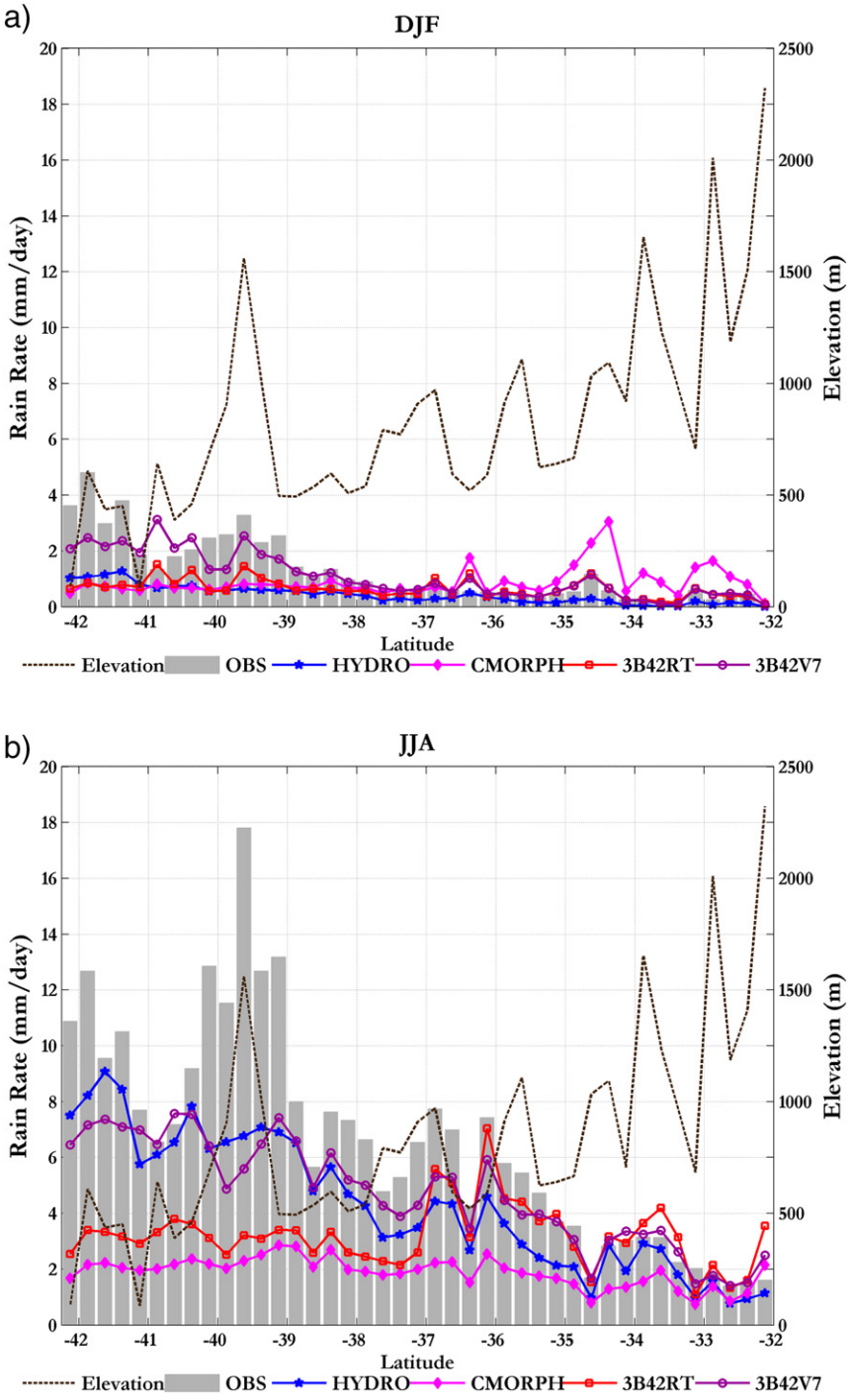

Fig. 5. Longitudinally averaged daily precipitation rates (mm day^{-1}) of observations and the various estimates of precipitation at the grid points available for the quarters (a) DJF and (b) JJA for the period 2004–2010 over the mountainous region of the subtropical Andes. The dotted line indicates the average elevation (m) considering the observed data points on each latitude.

indicates the percentage of the total precipitation that is explained for each interval of rain (relative rain volume) in dBR scale, and similarly in the shape of bars for the observed precipitation. Although each interval range of x-axis is 1 dBR, in accordance with Eq. (1), PDFs indicate the equivalent in mm day^{-1} of −10, 0, 10, 20 and 30 dBR (0.1, 1, 10, 100 and 1000 mm day^{-1} respectively), to better relate the percentages with the type of precipitation event. Thus, the curve of an estimate will agree with the observations in the extent that there exists an overlap between the two. In general, for data sets in a considerable period of time, these PDFs tend to a normal distribution in the dBR scale according to the central limit theorem (Amitai et al., 2009). In these graphs, the maximum contribution to the total volume of daily rainfall by surface observations is in the range 30 mm.

The curves of precipitation estimates in the PDFs are displaced to lower rainfall rates, with a greater contribution to the total volume by events of weak precipitation and the tendency to underestimate the events of intense precipitation. HYDRO presents the opposite behavior and a greater contribution from precipitation events around 40 mm. Total precipitation is underestimated in large proportion by all estimates, with CMORPH exemplifying this tendency with a total relation in the area of 0.48 and a maximum percentage contribution to the total volume of precipitation centered in 15 mm, unlike the distribution observed. The total ratio of 0.81 for 3B42 V7, along with a better agreement with the observed distribution confirm a major positive impact on this region from the changes made on this estimate. Although the estimate continues to understate the total rainfall in the area, its behavior improves over 3B42 RT. In line with the study of Salio et al. (2015), the results of the PDF, along with Table 2, represent the highlights of a daily evaluation of these satellite retrieved products over this mountainous region.

To analyze the latitudinal variation of estimates taking into account terrain elevation, Fig. 5 shows their behavior at the points where there is information available, with a longitudinal average of the daily precipitation values for seasonally warm and seasonally cold periods. The analysis of Fig. 8 considers the strong longitudinal contrast at different altitudes.

Fig. 5 shows a significant underestimation of the estimates at lower elevations in the southern region and an overestimation of some products at higher elevations in the northern region. In DJF, 3B42 V7 shows a favorable outcome south of 38°S reducing underestimation of rainfall compared to the rest of the products that underestimate rainfall in these latitudes. Further north, there is an overestimation of 3B42 RT and CMORPH, with larger overestimations with CMORPH. 3B42 V7 shows the best performance. HYDRO underestimates precipitation in summer throughout the latitudinal extension of the mountainous area. In JJA, HYDRO joins 3B42 V7 for the best performances in the

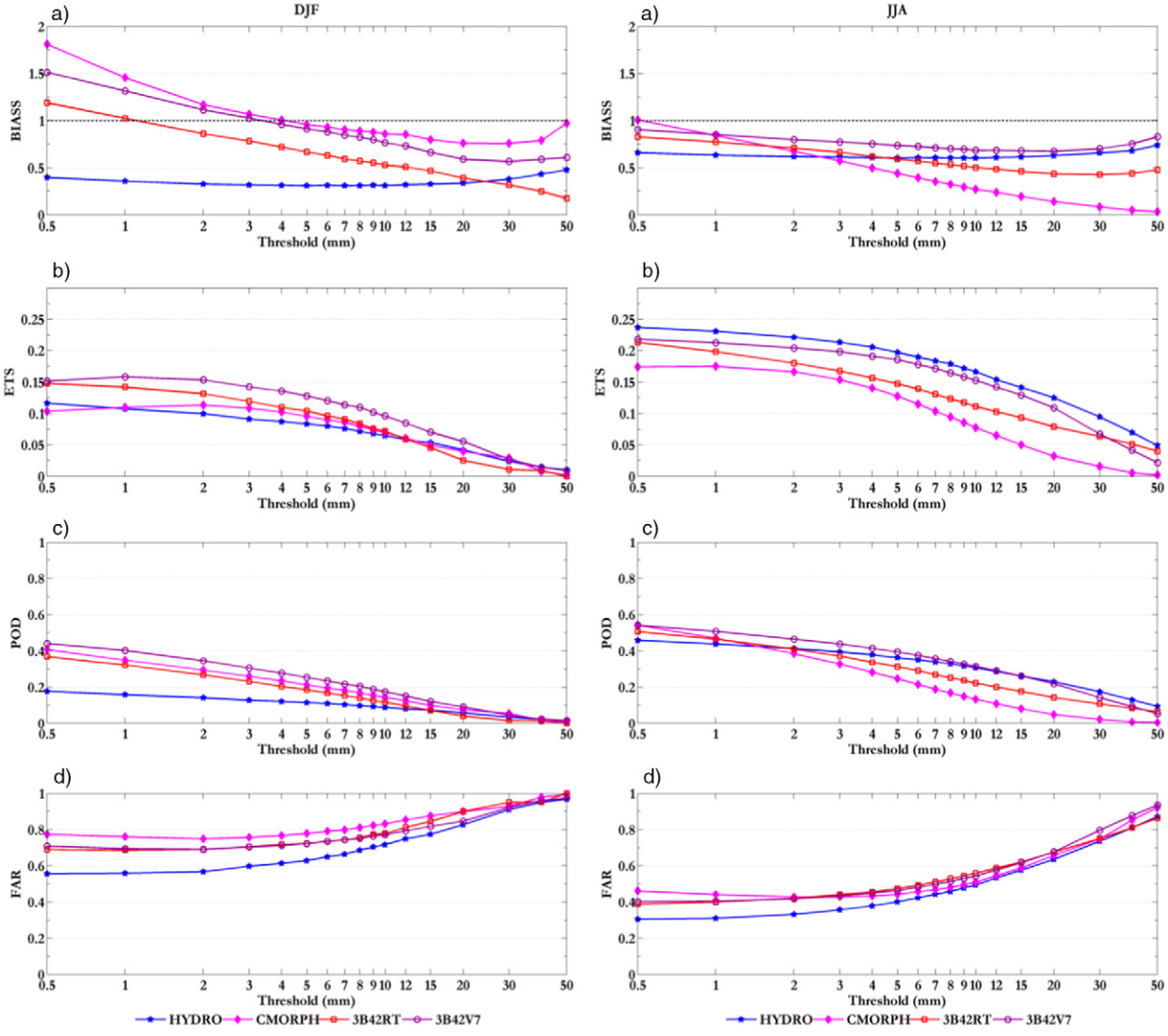

Fig. 6. (a) BIASS, (b) ETS, (c) POD and (d) FAR for the different rainfall estimates over the mountainous region of the subtropical Andes in the quarters DJF in the left panel, and JJA in the right panel for the period 2004–2010.

southern region, although both estimates remain below the observed values. North of 36°S, the estimates are closer to the observed precipitation, although 3B42 V7 and, in a larger extent 3B42 RT, show an overestimation in this season and for these latitudes. Meanwhile, CMORPH deviates below the observed values in winter and for all latitudes over this complex topography area.

The largest dependence of the error of rainfall estimates with topography is best observed in operational products. This is not the case for HYDRO, which underestimates in both seasons, with a better result in JJA, and is not affected by the terrain elevation. However, CMORPH in DJF and 3B42 RT in JJA maintain a significant underestimation in latitudes with lower terrain elevation and an overestimation at higher elevations.

This analysis shows the HYDRO competitiveness over this region despite using less information, and the limitations of PM data mainly in the case of CMORPH. The results indicate that in the southern region of the study area with rain gauges at low elevation, precipitation probably does not have a lot of ice crystals that allow the PM to improve the quality of 3B42 RT and CMORPH, whereas precipitation does seem to reach the cold brightness temperature threshold in the IR channel, allowing HYDRO to better approximate the observations. In turn, at higher elevations, solid precipitation could explain the overestimation of operational products with PM data. In the case of 3B42 V7, both the precipitation radar and rain gauge data show best fit values of precipitation. In the future, it is important to study the vertical profile of the precipitating clouds over this complex terrain region, in order to confirm this analysis about some of the differences found.

Fig. 6 confirms previous results (from Salio et al., 2015) where an improved performance in JJA was shown compared to DJF, and where the limitations of the estimates in this area were evidenced by the different statistical indices. Higher values of ETS and POD, and reduced false alarms in the winter confirm this result. 3B42 V7 shows an improvement in both seasons although it shows a large percentage of false alarms and to a lower extent underestimates precipitation over the region. In DJF, 3B42 V7 and CMORPH overestimate weak events and underestimate the most intense events above 4 mm but they achieve the best results compared to the other estimates. HYDRO has the largest underestimation in this quarter, which is also represented in the poor performance of the ETS and the POD, though not in false alarms in comparison with the other estimates. On the other hand, CMORPH does not perform well in the ETS, and has the highest degree of false alarms, and 3B42 RT shows an intermediate behavior. In JJA, a marked improvement in HYDRO appears in the result of all statistics, and the BIASS is observed to reduce, together with the 3B42 V7, the

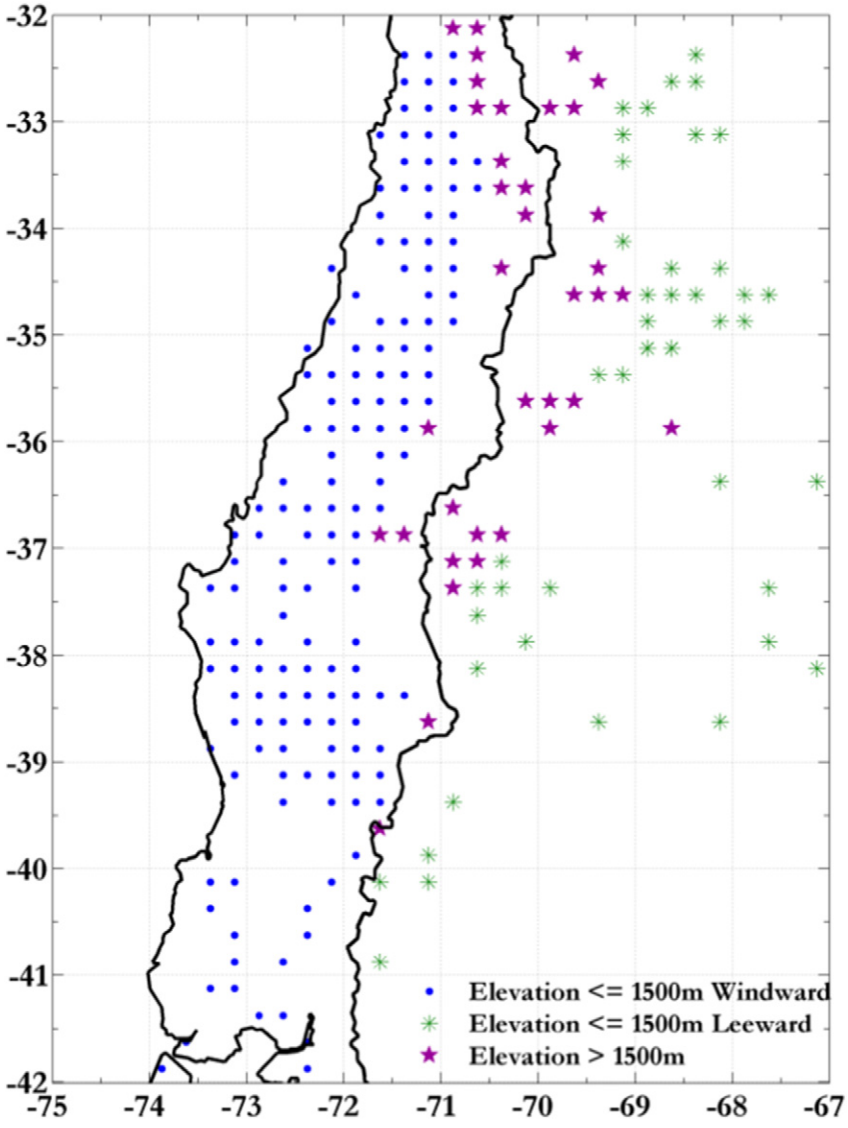

Fig. 7. Separation of the points available for validation depending on terrain elevation and location relative to the terrain.

underestimation that all products have principally in all the intense rainfall events. Furthermore, in comparison with the rest of the estimates, CMORPH performance worsens at this time of the year compared to the quarter DJF.

To contribute to the previous analysis, an analysis that takes into account the dependence of errors with terrain elevation was undertaken, separating the points available at a lower altitude with a maximum elevation of 1500 m, in the area upwind and downwind of the mountain range and high elevation points above 1500 m (Fig. 7). It is hence possible to evaluate the estimates taking into account the different types of events depending on the location relative to the orography.

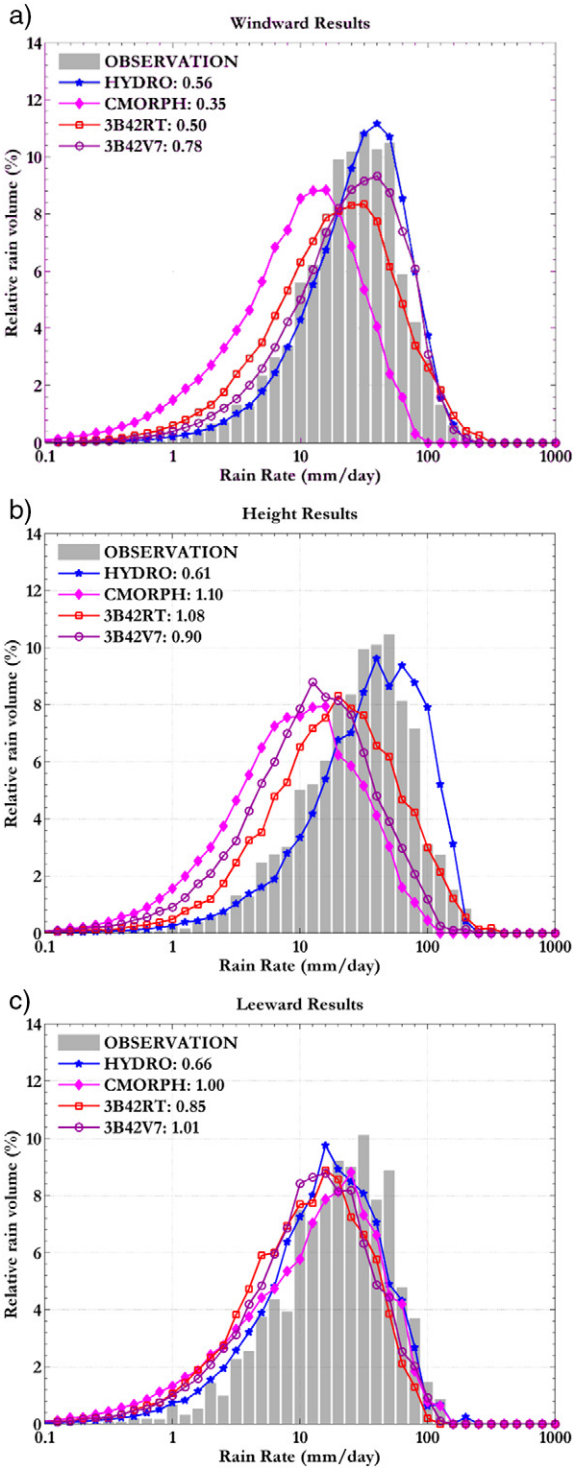

Fig. 8. PDFs for rainfall estimates during the entire study period, corresponding to (a) the windward area of the mountain range at a terrain elevation up to 1500 m, (b) the area at elevations above 1500 m, and (c) the leeward area of the mountain range at an elevation of land up to 1500 m.

Fig. 8 shows the results of the PDFs and Table 3 shows the values for CORR for different estimates of rainfall in the entire study period. The results indicate an added value to the analysis conducted throughout this work which started in Salio et al. (2015).

Fig. 8.a shows that for the points upwind of the Andes, where winter precipitation is very important, there is a marked underestimation of all estimates with respect to the rest of the areas defined in Fig. 7. This degree of underestimation is evident most clearly in the total relations of the PDF, and is most noticeable in CMORPH that has a displacement in its distribution towards lower precipitation intervals, with a total ratio of 0.35. In turn, it is observed that 3B42 V7 achieves better results in the PDF, both in the total ratio (0.78) and in its good correspondence with the observed distribution, and that HYDRO has the highest CORR in this case (Table 3). On the other hand, it is noted that the results for this area of the subtropical Andes dominates the result obtained in the PDF in Fig. 4. This is due to the greater number of points available and the development of more intense rainfall during the cold season in the windward side of the mountains, which is influenced mainly by atmospheric circulation in these latitudes, proximity to the sea and orographic forcing (Viale et al., 2013). In accordance with the physical processes and previous studies, the vast understatement in this area can relate to the warmer nature of the clouds windward, i.e., forced ascent of moist air can lead to cloud formation and development of precipitation with cloud top temperatures below brightness temperature thresholds in the IR channel algorithms and without sufficient ice crystals to be detected from microwave data (Viale and Garreaud, 2014).

For points at higher terrain elevations (elevations > 1500 m, Fig. 8.b) the correlation coefficient increases in all cases (Table 3), with the highest CORR at 0.42 for HYDRO and followed by 3B42 V7, except for CMORPH which obtains a very poor value. On the other hand, it is for terrain elevations above 1500 m that the greatest differences in the PDF appear between IR-only retrievals and those optimally combined with microwave data. CMORPH and the different 3B42 versions are displaced towards the lower thresholds of precipitation, while HYDRO appears slightly displaced to higher thresholds. It is important to note, however, that by analyzing the total relations, HYDRO shows the same underestimating behavior for total rainfall for all terrain elevations studied. At terrain elevations above 1500 m, CMORPH and 3B42 RT show total relations slightly higher than one. This is not observed in the remaining terrain elevation sub-sections of the region. The weak overestimation shown for operational products that include microwave data may be related to the limitations of these algorithms in regions with solid precipitation and snow-covered surfaces which are easily confused with precipitation. In this sense, 3B42 V7 which is adjusted with surface data, maintains a level of underestimation for precipitation due to the absence of operational rain gauges for calibration in this region(elevations > 1500 m), although not as prominent as in the windward area.

The analysis for the downwind area in Fig. 8.c shows similar result among all products considering that precipitation estimates are associated with the development of convective summer rainfall and an arid region in comparison with the rest of the areas selected. Correlation

Table 3
CORR values for different rainfall estimates in the entire study period, depending on the elevation of the terrain and location relative to the terrain. N represents the number of pairs observation-estimation available in each case for daily validation.

CORR	Windward $N = 378.410$	Height $N = 90.824$	Leeward $N = 107.038$
HYDRO	0,35	0,42	0,31
CMORPH	0,31	0,14	0,28
3B42 RT	0,29	0,34	0,29
3B42 V7	0,32	0,37	0,33

values in Table 3 are high for 3B42 V7 which has rain gauge data calibration. Similarly, the PDF shows a good correspondence between all the distributions and the observed distribution. Total precipitation relations improve in this area compared to other sectors with a marked proximity to one in all cases. Although in this case the limitation linked to the evaporation of precipitation dominates below the cloud base, as discussed previously, it is further shown that satellite based precipitation estimates reduce the errors in convective precipitation cases.

6. Study cases

To complete this work, the analysis of two cases of intense precipitation for the year 2014 is here presented. The year 2014 marked the start of the GPM era, which allows including IMERG final run (IMERG FR) in comparison with 3B42 V7, the product which obtained best results in the previous analysis. The daily precipitation data available over this region were used and compared with the closest in each grid point. The two events are characterized by high values of daily precipitation but differ in their meteorological development, one more closely linked to the development of convective precipitation in the summer season in April 2014 (Fig. 9), and the other associated with the development of orographic precipitation more closely linked to the winter season in June 2014 (Fig. 10).

In the analysis of the April 8th, 2014 event in Fig. 9, although there is a low density of available stations on the Argentine side, correspondence is observed in the precipitant areas with the precipitation fields estimated by IMERG FR and 3B42 V7. Both estimates show in the northern area an increase in precipitation on the highest slopes of the mountains (see Fig. 1) and a reduced precipitation downwind of them in coincidence with observations. Similar to rain gauge data, rainfall estimates are observed to concentrate the most of precipitation in the southeast of the region of interest. In volumetric PDFs, estimates are observed to slightly overestimate the observed distribution, both in the total ratios shown to be above one, as well as in the displacement of the precipitation curves towards higher thresholds of precipitation. This result is slightly higher for IMERG FR, and is also reflected in the value of its BIAS (not normalized in these study cases), and in the average and maximum statistical values. However, both in scatter plots, as well as in most of the indices used, an improvement is observed in IMERG FR which reduces the average error, increases the degree of linear association with observations, and has better results in categorical statistics. In this regard, the analysis of this convective case associated with summer rainfall over this region, reveals a reduction in the level of underestimation of rain and an improvement in the values of the various indices by IMERG FR with respect to the results of 3B42 V7 analyzed throughout this work and previous studies.

The analysis of the June 11th 2014 event is shown in Fig. 10. This case study relies on a greater amount of surface information to compare with estimates. Both estimates coincide in the area of the observed precipitation, and IMERG FR results in a better match with the observed values. The 3B42 V7 precipitation field has a maximum daily precipitation over 150 mm which is not seen in the observed field, and it also extends

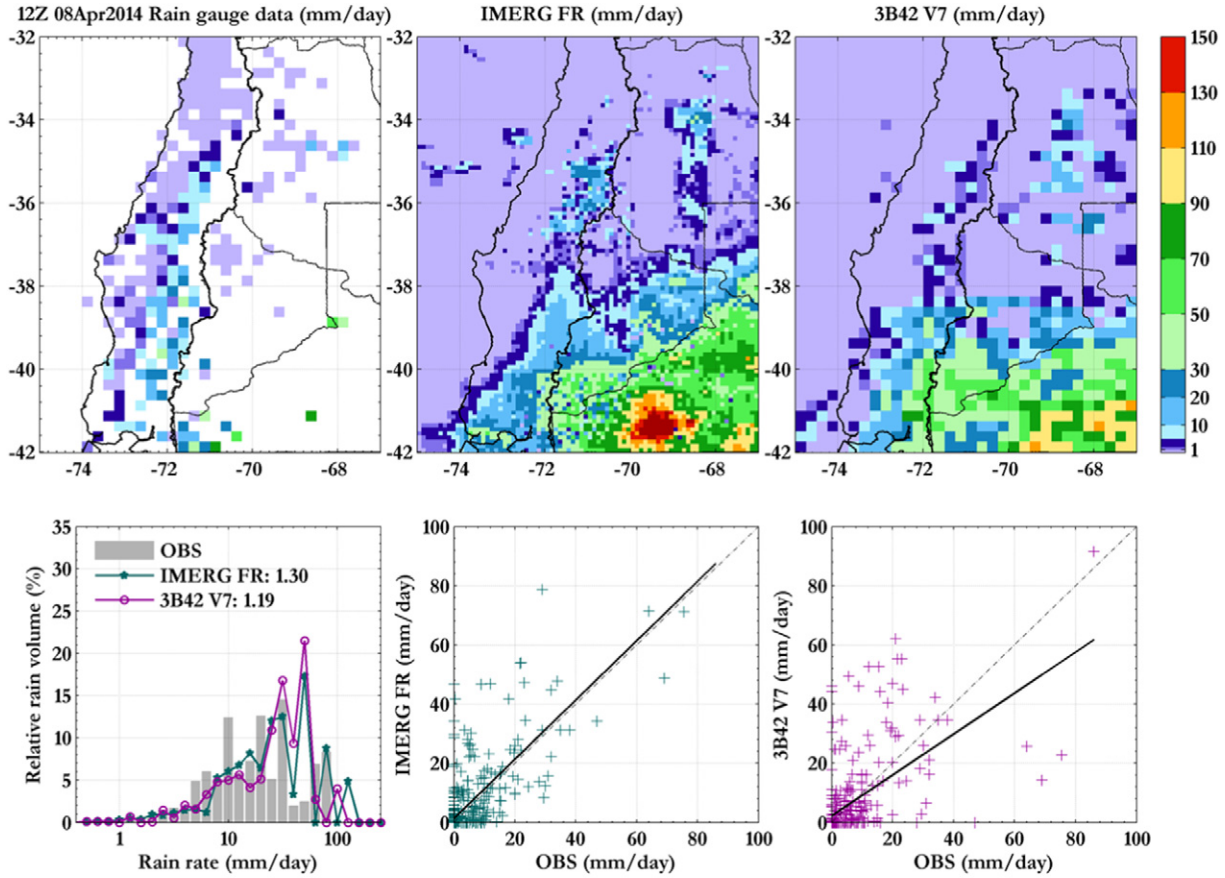

N=437	AVG (OBS=4.44)	MAX (OBS=86.00)	RMSE	BIAS	CORR	ETS	BIASS	POD	FAR
IMERG FR	5,78	122.54	8.32	1.33	0.77	0.38	0.94	0.71	0.25
3B42 V7	5.27	91.57	10.25	0.83	0.57	0.40	0.81	0.66	0.18

Fig. 9. 24 hour accumulated precipitation comparison at 12 UTC on April 8th, 2014: observed rainfall (upper left panel), estimated by IMERG FR (upper central panel) and estimated by 3B42 V7 (upper right panel), volumetric PDFs (bottom left panel), scatter plot for IMERG FR (bottom central panel), and for 3B42 V7 (lower right panel) and statistical totals (table). N represents the number of observation-estimate pairs available. Categorical indices are calculated for the threshold of 1 mm.

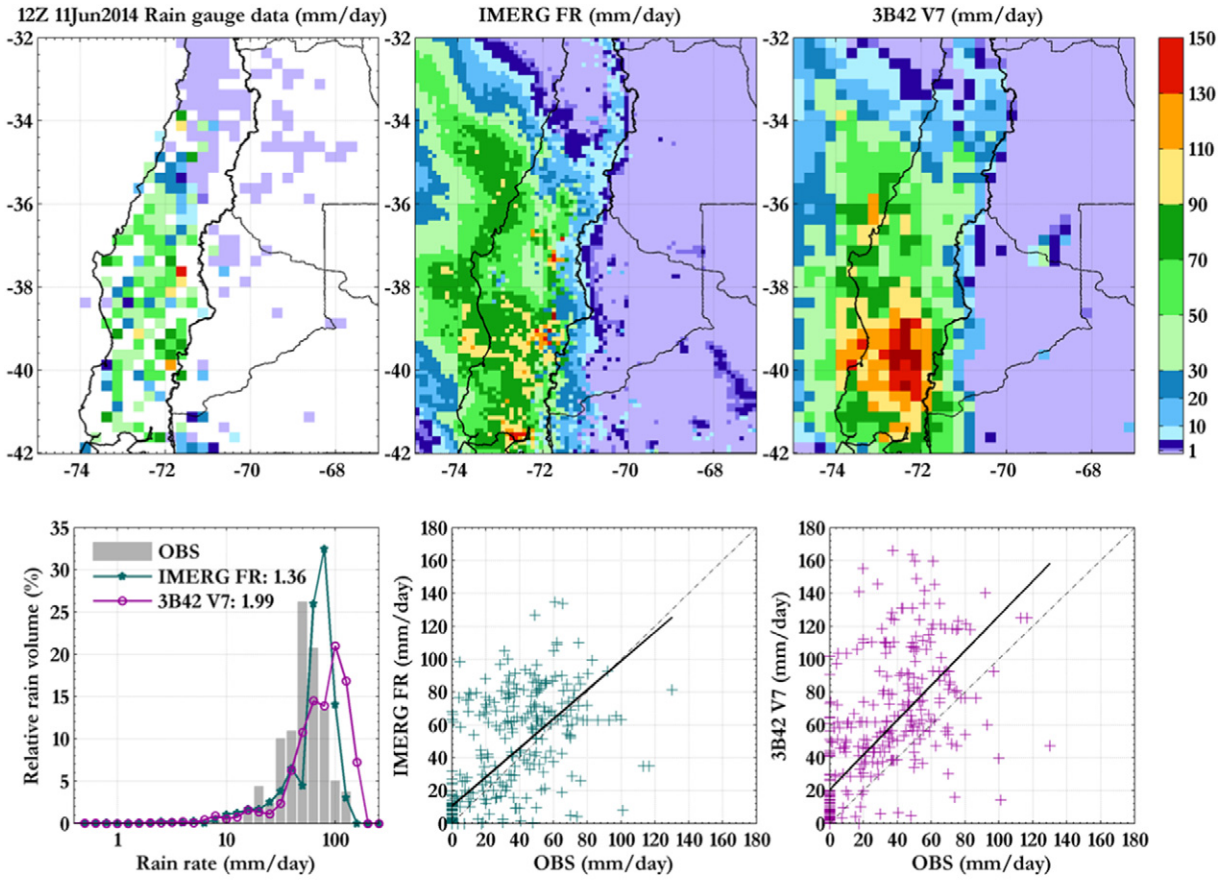

N=437	AVG (OBS=22.03)	MAX (OBS=130.00)	RMSE	BIAS	CORR	ETS	BIASS	POD	FAR
IMERG FR	30.04	134.66	25.09	8.01	0.71	0.47	1.29	0.97	0.25
3B42 V7	43.89	166.07	37.12	21.85	0.69	0.20	1.62	1.00	0.39

Fig. 10. Idem Fig. 9 for June 11th, 2014.

to the north and to the south the higher values of precipitation, obtaining an overestimation of rain that is not observed for IMERG FR. In the volumetric PDFs, this performance is corroborated with a noticeable difference in the degree of overestimation far superior in 3B42 V7, both in the overall relation, as well as in the shift to higher thresholds of precipitation. In this situation of intense precipitation, both the scatter plots and in all statistical indicators, the improved performance of IMERG FR with respect to 3B42 V7 is shown. Although, there is a degree of overestimation compared to observations, the results of the various indices indicate the better quality of the IMERG FR estimate.

In the analysis of these cases, the difficulties of the estimates in this region of complex terrain are observed, but advances are also shown in the newest product to optimize satellite precipitation estimation. As previously mentioned, the availability of IMERG reprocessed data covering previous years in the future will allow a daily validation on this area considering a longer period of time and to robustly assess the benefits of using more current GPM derived data over the subtropical Andes.

7. Conclusions

The present work conducted an assessment of different daily precipitation estimates over the subtropical Andes, focusing the analysis on areas of complex topography and their main differences between DJF and JJA. Such areas represent a challenge for satellite-derived data, and the scarcity of weather stations in such a remote area conditions the evaluation of the available data.

In accordance with Salio et al. (2015), and significantly extending the validation period, those estimates that include microwave data were found to be of better quality than HYDRO estimates. In turn, their adjustment with rain gauge data (3B42 V7 and IMERG FR) improved performance. Modifications to 3B42 V7 were favorable with respect to the performance of 3B42 RT. The results also indicated a better performance of estimates in the coldest and wettest season JJA, and a significant underestimation of precipitation throughout the year, which is most prominent in CMORPH.

The analysis taking into account the average terrain elevation shows an underestimation of the estimates to low land elevation and overestimation at higher altitudes. HYDRO estimates based on IR data do not show a dependency of the errors with the topography like CMORPH and 3B42 RT which use microwave data. In this sense, HYDRO underestimates precipitation throughout the latitudinal extension in DJF and improves its performance in JJA without large variations with latitude. Instead, CMORPH in DJF and 3B42 RT in JJA show an overestimation to the north and at higher terrain elevations and an underestimation to the south. In turn, CMORPH markedly underestimates precipitation throughout the area for the wettest JJA quarter and 3B42 V7 has better results in both seasons.

Categorical indices based on the different thresholds used indicate in DJF a large overestimation of CMORPH for events of weak precipitation. The least optimal results for this summer quarter correspond to HYDRO, being the most notorious in underestimating a large percentage of precipitation at all thresholds. 3B42 V7 performed better in comparison with the other estimates analyzed. In JJA, HYDRO reduces the level of underestimation together with 3B42 V7, mainly in the most intense precipitating events, and CMORPH presents the most unfavorable results.

The analysis taking into account the dependence of errors with terrain elevation, showed a marked level of underestimation windward of the terrain, which could be associated with the development of precipitation from warmer and relatively lower clouds. On the other hand, a slight overestimation is shown at points located at higher elevations for data estimates using microwave data. This result could be linked to the limitations of these products in areas covered by snow. Finally, the best estimate performances were found downwind of the terrain, where the nature of convective precipitation reduces errors in satellite estimates.

In the future, it is necessary to generate correction factors considering areas of solid precipitation and temperature thresholds appropriate to the nature of clouds in mountainous regions. Following the launch of the GPM mission, the quality of the new IMERG research product in its FR version was evaluated for two intense precipitating events. This analysis resulted in more optimal values in the statistical indices, which decreases the degree of underestimation exposed in this work and previous studies on the region. Nevertheless, there is an overestimation of precipitation in the most extreme events that should be taken into account. The influence of solid precipitation and drier areas in the outcome of these estimated data should be assessed. It is thus necessary to perform a validation of the IMERG data as it becomes available for a more extended period of time.

Acknowledgments

The present work was supported by the projects from Argentina PIDDEF 47/2010, PIDDEF 16/2014, ANPCyT PICT 2013-1299, UBACyT 20020130100618BA, CONICET - CNPQ International cooperation project 2699-12 and 1793-13 and ALERT.AR Argentinean cooperation project. Data was provided by the following institutions: Servicio Meteorológico Nacional - Argentina; Subsecretaría de Recursos Hídricos de la Nación - Argentina; Autoridad Interjurisdiccional del Agua - Neuquén - Argentina; Instituto Nacional de Tecnología Agropecuaria - Argentina; and Dirección General de Aguas - Chile.

References

Amitai, E., Lord, X., Sempere-Torres, D., 2009. Comparison of TRMM radar rainfall estimates with NOAA next generation QPE. J. Meteorol. Soc. Jpn. 87A, 109–118.
Amitai, E., Petersen, W., Llort, X., Vasiloff, S., 2012. Multiplatform comparisons of rain intensity for extreme precipitation events. IEEE Trans. Geosci. Remote Sens. 50 (3): 675–686. http://dx.doi.org/10.1109/TGRS.2011.2162737.
Blacutt, L.A., Dirceu, L.H., de Gonçalves, L.G.G., Vila, D.A., Andrade, M., 2015. Precipitation comparison for the CFSR, MERRA, TRMM3B42 and combined scheme datasets in Bolivia. 6th WIPWG Special Issue Atmospheric Research. 163:pp. 117–131. http://dx.doi.org/10.1016/j.atmosres.2015.02.002.
Demaria, E.M.C., Rodriguez, D.A., Ebert, E.E., Salio, P., Su, F., Valdes, J.B., 2011. Evaluation of mesoscale convective systems in South America using multiple satellite products and an object-based approach. J. Geophys. Res. 116, D08103. http://dx.doi.org/10.1029/2010JD015157.
Dinku, T., Chidzambwab, S., Ceccatoa, P., Connora, S.J., Ropelewskia, C.F., 2008. Validation of high-resolution satellite rainfall products over complex terrain. Int. J. Remote Sens. 29 (14), 4097–4110.
Dinku, T., Ruiz, F., Connor, S.J., Ceccato, P., 2010. Validation and intercomparison of satellite rainfall estimates over Colombia. J. Appl. Meteorol. Climatol. 49 (5), 1004–1014.
Dinku, T., Ceccato, P., Connor, S.J., 2011. Challenges of satellite rainfall estimation over mountainous and arid parts of east Africa. Int. J. Remote Sens. 32 (21), 5965–5979.
Ebert, E.E., Janowiak, J.E., Kidd, C., 2007. Comparison of near-real-time precipitation estimates from satellite observations and numerical models. Bull. Am. Meteorol. Soc. 88:47–64. http://dx.doi.org/10.1175/BAMS-88-1-47.
Gao, Y.C., Liu, M.F., 2012. Evaluation of high-resolution satellite precipitation products using rain gauge observations over the Tibetan Plateau. Hydrol. Earth Syst. Sci. Discuss. 9, 9503–9532.
Garreaud, R., 2013. Warm winter storms in central Chile. J. Hydrometeorol. 14: 1515–1534. http://dx.doi.org/10.1175/JHM-D-12-0135.1.
Habib, E., El Saadani, M., Haile, A.T., 2012. Climatology-focused evaluation of CMORPH and TMPA satellite rainfall products over the Nile Basin. J. Appl. Meteorol. Climatol. 51 (12), 2105–2121.
Hirpa, F.A., Gebremichael, M., Hopson, T., 2010. Evaluation of high-resolution satellite precipitation products over very complex terrain in Ethiopia. J. Appl. Meteorol. Climatol. 49 (5), 1044–1051.
Huffman, G.J., Bolvin, D.T., Nelkin, E.J., Wolff, D.B., Adler, R.F., Gu, G., Hong, Y., Bowman, K.P., Stocker, E.F., 2007. The TRMM multisatellite precipitation analysis (TMPA): quasi-global, multiyear, combined-sensor precipitation estimates at fine scales. J. Hydrometeorol. 8:38–55. http://dx.doi.org/10.1175/JHM560.1.
Huffman, G.J., Bolvin, D.T., 2014. TRMM and Other Data Precipitation Data Set Documentation, Lab. for Atmos. NASA Goddard Space Flight Center and Science Systems and Applications ftp://precip.gsfc.nasa.gov/pub/trmmdocs/3B42_3B43_doc.pdf (accessed 15.11.01).
Huffman, G.J., Bolvin, D.T., Nelkin, E.J., 2015. Integrated Multi-satellitE Retrievals for GPM (IMERG) Technical Documentation. NASA/GSFC Code 612, 47. http://pmm.nasa.gov/sites/default/files/document_files/IMERG_doc.pdf (accessed 16.09.19).
Joyce, R.J., Janowiak, J.E., Arkin, P.A., Xie, P., 2004. CMORPH: a method that produces global precipitation estimates from passive microwave and infrared data at high spatial and temporal resolution. J. Hydrometeorol. 5:487–503. http://dx.doi.org/10.1175/1525-7541(2004)005<0487:CAMTPG>2.0.CO;2.
Kidd, C., Levizzani, V., 2011. Status of satellite precipitation retrievals. Hydrol. Earth Syst. Sci. 15, 1109–1116.
Kucera, P.A., Ebert, E.E., Turk, F.J., Levizzani, V., Kirschbaum, D., Tapiador, F.J., Loew, A., Borsche, M., 2013. Precipitation from space: advancing earth system science. Bull. Am. Meteorol. Soc. 94:365–375. http://dx.doi.org/10.1175/BAMS-D-11-00171.1.
Liebmann, B., Allured, D., 2005. Daily precipitation grids for South America. Bull. Am. Meteorol. Soc. 86:1567–1570. http://dx.doi.org/10.1175/BAMS-86-11-1567.
Liu, C., Zipser, E.J., 2009. "Warm rain" in the tropics: seasonal and regional distributions based on 9 yr of TRMM data. J. Climatol. 22:767–779. http://dx.doi.org/10.1175/2008JCLI2641.1.
Nurmi, P., 2003. Recommendations on the verification of local weather forecasts. ECMWF Tech. Memo. N. 430 (19pp).
Okamoto, K., Iguchi, T., Takahashi, N., Iwanami, K., Ushio, T., 2005. The global satellite mapping of precipitation (GSMaP) project. 25th IGARSS Proceedings, pp. 3414–3416.
Porcu, F., Milani, L., Petracca, M., 2014. On the uncertainties in validating satellite instantaneous rainfall estimates with raingauge operational network. Atmos. Res. 144: 73–81. http://dx.doi.org/10.1016/j.atmosres.2013.12.007.
Rosenfeld, D., Woodley, W.L., Krauss, T.W., Makitov, V., 2006. Aircraft microphysical documentation from cloud base to anvils of hailstorm feeder clouds in Argentina. J. Appl. Meteorol. Climatol. 45:1261–1281. http://dx.doi.org/10.1175/JAM2403.1.
Ruiz, J.J., 2009. Evaluation of different methodologies to calibrate CMORPH over South America. Revista Brasileira de Meteorologia 24 (4), 473–488.
Salio, P., Hobouchian, M.P., García Skabar, Y., Vila, D., 2015. Evaluation of high-resolution satellite precipitation estimates over Southern South America using a dense rain gauge network. 6th WIPWG Special Issue Atmospheric Research. 163:pp. 146–161. http://dx.doi.org/10.1016/j.atmosres.2014.11.017.
Sanchez, J.L., Gil-Robles, B., Dessens, J., Martin, E., Lopez, L., Marcosa, J.L., Berthetb, C., Fernández, J.T., García-Ortega, E., 2011. Characterization of hailstone size spectra in hailpad networks in France, Spain, and Argentina. Atmos. Res. 93 (1–3), 641–654.
Scofield, R.A., Kuligowski, R.J., 2003. Status and outlook of operational satellite precipitation algorithms for extreme-precipitation events. Weather Forecast. 18:1037–1051. http://dx.doi.org/10.1175/1520-0434(2003)018<1037:SAOOOS>2.0.CO;2.
Sorooshian, S., Hsu, K.L., Gao, X., Gupta, H.V., Imam, B., Braithwaite, D., 2000. Evaluation of PERSIANN system satellite-based estimates of tropical rainfall. Bull. Am. Meteorol. Soc. 81:2035–2046. http://dx.doi.org/10.1175/1520-0477(2000)081<2035:EOPSSE>2.3.CO;2.
Su, F., Hong, Y., Lettenmaier, D.P., 2008. Evaluation of TRMM multisatellite precipitation analysis (TMPA) and its utility in hydrologic prediction in the La Plata Basin. J. Hydrometeorol. 9 (4), 622–640.
Tapiador, F.J., Turk, F.J., Petersen, W., Hou, A.Y., García-Ortega, E., Machado, L.A.T., Angelis, C.F., Salio, P., Kidd, C., Huffman, G.J., De Castro, M., 2012. Global precipitation measurement: methods, datasets and applications. Atmos. Res. 104–105, 70–97.
Viale, M., Nuñez, M.N., 2011. Climatology of winter orographic precipitation over the Subtropical Central Andes and associated synoptic and regional characteristics. J. Hydrometeorol. 12:481–507. http://dx.doi.org/10.1175/2010JHM1284.1.
Viale, M., Houze Jr., R.A., Rasmussen, K.L., 2013. Upstream orographic enhancement of a narrow cold-frontal rainband approaching the Andes. Mon. Weather Rev. 141: 1708–1730. http://dx.doi.org/10.1175/MWR-D-12-00138.1.
Viale, M., Garreaud, R., 2014. Summer precipitation events over the western slope of the Subtropical Andes. Mon. Weather Rev. 142:1074–1092. http://dx.doi.org/10.1175/MWR-D-13-00259.1.
Vicente, G., Scofield, R., Davenport, J., 2001. The role of orographic and parallax corrections on real time high resolution satellite rainfall rate distribution. Int. J. Remote Sens. 23 (2), 221–230.
Vila, D.A., Scofield, R.A., Davenport, J., 2002. Satellite rainfall estimation over South America: evaluation of two major events. AMS 16th Conference on Hydrology, pp. 33–36.
Vila, D.A., De Goncalves, L., Toll, D.L., Rozante, J.R., 2009. Statistical evaluation of combined daily gauge observations and rainfall satellite estimates over continental South America. J. Hydrometeorol. 10:533–543. http://dx.doi.org/10.1175/2008JHM1048.1.
Zipser, E.J., Cecil, D.J., Liu, C., Nesbitt, S.W., Yorty, D.P., 2006. Where are the most intense thunderstorms on Earth? Bull. Am. Meteorol. Soc. 87, 1057–1071.